Synthetic recombinant bat SARS-like coronavirus is infectious in cultured cells and in mice

Michelle M. Becker[a,1], Rachel L. Graham[b,1], Eric F. Donaldson[b], Barry Rockx[b], Amy C. Sims[b,c], Timothy Sheahan[b], Raymond J. Pickles[d,e], Davide Corti[f], Robert E. Johnston[c], Ralph S. Baric[b,c,d,2], and Mark R. Denison[a,g,2]

Departments of [a]Pediatrics and [g]Microbiology and Immunology, Vanderbilt University, Nashville, TN 37232; Departments of [b]Epidemiology and [d]Microbiology and Immunology, [e]Cystic Fibrosis/Pulmonary Research and Treatment Center and Department of Medicine, and [c]Carolina Vaccine Institute, University of North Carolina, Chapel Hill, NC 27599; and [f]Institute for Research in Biomedicine, CH-6500 Bellinzona, Switzerland

Edited by Peter Palese, Mount Sinai School of Medicine, New York, NY, and approved October 14, 2008 (received for review August 18, 2008)

Defining prospective pathways by which zoonoses evolve and emerge as human pathogens is critical for anticipating and controlling both natural and deliberate pandemics. However, predicting tenable pathways of animal-to-human movement has been hindered by challenges in identifying reservoir species, cultivating zoonotic organisms in culture, and isolating full-length genomes for cloning and genetic studies. The ability to design and recover pathogens reconstituted from synthesized cDNAs has the potential to overcome these obstacles by allowing studies of replication and pathogenesis without identification of reservoir species or cultivation of primary isolates. Here, we report the design, synthesis, and recovery of the largest synthetic replicating life form, a 29.7-kb bat severe acute respiratory syndrome (SARS)-like coronavirus (Bat-SCoV), a likely progenitor to the SARS-CoV epidemic. To test a possible route of emergence from the noncultivable Bat-SCoV to human SARS-CoV, we designed a consensus Bat-SCoV genome and replaced the Bat-SCoV Spike receptor-binding domain (RBD) with the SARS-CoV RBD (Bat-SRBD). Bat-SRBD was infectious in cell culture and in mice and was efficiently neutralized by antibodies specific for both bat and human CoV Spike proteins. Rational design, synthesis, and recovery of hypothetical recombinant viruses can be used to investigate mechanisms of transspecies movement of zoonoses and has great potential to aid in rapid public health responses to known or predicted emerging microbial threats.

emerging pathogens | synthetic biology | vaccine development | zoonoses

Emergence of zoonotic-human pathogens is increasingly recognized as a threat to public health (1). Human population growth and environmental changes have created new opportunities for contact between humans and zoonotic organisms that may result in cross-species transmission and human disease (1, 2). Recent examples include RNA viruses such as severe acute respiratory syndrome coronavirus (SARS-CoV), Ebola, Hanta, Nipah, and Chikungunya viruses (2). However, the determinants regulating successful transspecies movement remain poorly understood due to challenges in identifying viral precursors and animal reservoirs, thereby complicating vaccine and therapeutic design (3). SARS-CoV, which exemplifies the challenges inherent in studying emerging pathogens, was the first 21st century emerging virus to exhibit efficient human-to-human transmission and rapid global spread (4–6). Although zoonotic SARS-CoV strains were isolated from civets and raccoon dogs (7–9), the epidemic likely originated from strains circulating in bats (Bat-SCoVs) (10–12). Bat CoVs cluster in both major mammalian CoV taxonomic groups, raising the possibility that Bat CoVs may be progenitors to all 4 known pathogenic human CoVs (11, 13). Bats are also predicted to function as reservoirs for other important emerging human and animal viruses (14, 15). Although several complete Bat CoV genome sequences are available, no Bat CoV has been successfully cultivated in cell culture or in animals (11, 13), severely limiting the identification of determinants of zoonotic CoV transspecies movement.

The SARS-CoV Spike is a 180-kDa type I membrane glycoprotein that contains a well-defined receptor-binding domain (RBD). The SARS-CoV genome is likely a mosaic of sequences derived from multiple recombination events, although this hypothesis is somewhat controversial (16). However, recombination within Spike has been described often (17), suggesting that the RBDs may be interchangeable between strains (18–20). During the SARS-CoV outbreak, evolution in the Spike RBD allowed for more efficient use of human angiotensin-converting enzyme 2 (hACE2) as a receptor for entry (21, 22). Because future zoonoses are likely, it is critical to identify strategies used by viruses to adapt in human populations. In this study, we have combined phylogenetic and bioinformatics analyses, large-scale cDNA synthesis, chimeric gene design, and reverse genetics to generate a consensus Bat-SCoV. Successful recovery of the infectious chimeric virus, Bat-SRBD, which includes the RBD within Spike from human SARS-CoV, demonstrates the plasticity of the CoV type I glycoprotein. The synthetic reconstruction and recovery of this novel chimeric virus identifies a necessary genetic element for CoV cross-species transmission, establishes a model system for testing experimental evolution of zoonotic CoVs, and allows for testing of vaccine and therapeutics against possible future zoonotic strains.

Results

Consensus Bat-SCoV Sequence Design and Construction. When this study was initiated, 4 Bat-SCoVs had been identified (HKU3–1, HKU3–2, HKU3–3, and RP3) as the virus reservoir populations from which SARS-CoV emerged (10–12). Because none had been recovered in culture, the infectivity of the reported viral genomic RNA sequences was hypothetical, having been derived from RT-PCR sequencing of bat fecal or rectal swab samples. Sequence databases have error frequencies from 1/500 to 1/10,000, making viable genome reconstruction problematic with increasing size (23). Therefore, we used the 4 reported Bat-SCoV sequences to establish a putative consensus Bat-SCoV sequence (GenBank accession no. FJ211859) and designed cDNA fragments with junctions precisely aligned to the existing SARS-CoV reverse genetics system [Fig. 1*A*; supporting information (SI) Fig. S1] (24). The defined and functional SARS-CoV 5′ UTR and transcriptional regulatory sequences

Author contributions: M.M.B., R.L.G., E.F.D., R.S.B., and M.R.D. designed research; M.M.B., R.L.G., E.F.D., B.R., and A.C.S. performed research; R.L.G., E.F.D., T.S., R.J.P., D.C., and R.E.J. contributed new reagents/analytic tools; M.M.B., R.L.G., E.F.D., B.R., A.C.S., R.J.P., and R.S.B. analyzed data; and M.M.B., R.L.G., R.S.B., and M.R.D. wrote the paper.

Conflict of interest statement: R.E.J. is a coinventor of the Venezuelan Equine Encephalitis (VEE) expression vector technology and holds an equity interest in AlphaVax, Inc., the company that has licensed this technology from the University of North Carolina.

This article is a PNAS Direct Submission.

Freely available online through the PNAS open access option.

Data deposition: The sequences reported in this paper have been deposited in the GenBank database (accession nos. FJ211859 and FJ211860).

[1]M.M.B and R.L.G. contributed equally to this work.

[2]To whom correspondence may be addressed. E-mail: rbaric@email.unc.edu or mark.denison@vanderbilt.edu.

This article contains supporting information online at www.pnas.org/cgi/content/full/0808116105/DCSupplemental.

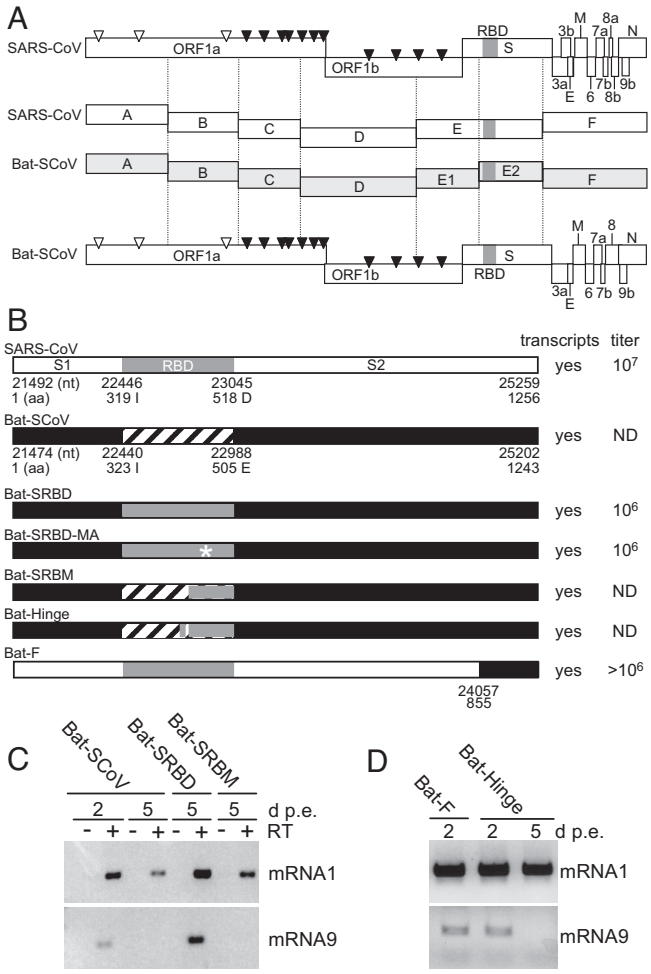

Fig. 1. Schematic representation of SARS-CoV and Bat-SCoV variants. (*A*) Schematic representation of SARS-CoV and Bat-SCoV (GenBank accession no. FJ211859) genomes and reverse genetics system. (*Top*) Arrowheads indicate nsp processing sites within the ORF1ab polyprotein (open arrowheads, papain-like proteinase mediated; filled arrowheads, nsp5 [3C-like proteinase] mediated). Immediately below are the fragments used in the reverse genetics system, labeled A through F. The fragments synthesized to generate Bat-SCoV exactly recapitulate the fragment junctions of SARS-CoV with the exception that the Bat-SCoV has 2 fragments, Bat-E1 and Bat-E2, which correspond to the SARS-E fragment. (*B*) Schematic representation showing organization of the SARS-CoV and Bat-SCoV Spike proteins. The engineered Spike proteins are pictured below with the virus name to the left. Bat-SRBD includes all of the Bat-SCoV Spike sequence except that the Bat-SCoV RBD (Bat-SCoV amino acid 323–505) is replaced with the SARS-CoV RBD (amino acid 319–518) (GenBank accession no. FJ211860). Bat-SRBD-MA includes the MA15 Spike RBD change at SARS-CoV aa Y436H. Bat-SRBM includes the minimal 13 SARS-CoV residues critical for ACE2 contact, resulting in a chimeric RBD of Bat-SCoV amino acid 323I-429T and SARS-CoV amino acid 426R-518D. Bat-Hinge is Bat-SRBM sequence, with Bat-SCoV amino acid 392L-397E replaced with SARS-CoV amino acid 388V-393D. Bat-F includes nt 1–24057 of SARS-CoV (to Spike amino acid 855), with the remaining 3′ sequence from Bat-SCoV. To the right of the schematic representations, observation of transcript activity and approximate stock titers at passage 1 (P1) are indicated. ND indicates no infectious virus detected by plaque assay. (*C* and *D*) Presence of genomic and subgenomic transcripts after electroporation of in vitro transcribed viral RNA. Band corresponding to mRNA1 indicates the presence of genomic RNA, either electroporated genomic RNA or progeny genomic RNA, and the presence of a band corresponding to mRNA9 indicates the presence of leader-containing subgenomic RNA, consistent with mRNA transcription.

were used because the 5′ UTRs of the Bat-SCoVs were incomplete. The genomic cDNA fragments were commercially synthesized, inserted into vectors, assembled into a full-length cDNA, and transcribed in vitro to yield genomic RNA. Initial attempts to recover and passage infectious Bat-SCoV failed. Electroporated cells contained high levels of genome and leader-containing subgenomic transcripts on day 2, but not day 5 postelectroporation (p.e.) (Fig. 1*C*), indicating that the synthetic consensus Bat-SCoV genome expressed a functional replicase. We did recover infectious virus consisting of SARS-CoV genome fragments A–E and Bat fragment F (Fig. 1 *B* and *D*). The resulting virus, Bat-F, encoded a chimeric Spike. Thus, the amino-terminal two-thirds of SARS-CoV Spike, including the RBD, and the fusion core contained within the carboxyl-terminal third of Bat-SCoV Spike can successfully drive productive infection. Also, because Bat-F contained Bat-SCoV accessory and structural genes 3′ to the Spike gene, these downstream ORFs are clearly interchangeable.

Generation and Recovery of Chimeric Bat-SRBD. The ectodomain of Spike can be exchanged among CoVs, altering host-range specificity (25, 26). To test whether the RBDs of Bat-SCoV and SARS-CoV were interchangeable, we replaced the Bat-SCoV RBD (amino acid 323–505) with the SARS-CoV RBD (amino acid 319–518) (27, 28) (GenBank accession no. FJ211860), simulating a theoretical recombination event that might occur during mixed infection in vivo (Fig. 1*B*). After electroporation, Bat-SRBD genome RNA and leader-containing subgenomic mRNA transcripts were detected (Fig. 1*C*), and progeny virions were detected by plaque assay. After 2 additional passages, the population genome sequence was identical to the Bat-SRBD molecular clone. However, 4 nucleotides exhibited dual peaks on the sequencing electropherograms, suggesting quasispecies variation at these positions (Table S1). Recovery and passage of Bat-SRBD demonstrated the functional interchangeability of human and animal SARS-CoV-like RBDs.

The crystal structure of SARS-CoV RBD complexed with its receptor, hACE2 (29), implicated 13 residues within the carboxyl terminus of the RBD (amino acid 426R-518D) in ACE2 engagement. Homology modeling indicated that this receptor-binding motif (RBM) may be sufficient to allow ACE2 engagement, and further predicts that inclusion of 6 residues amino-terminal to the RBM (amino acid 388V-393D) may enhance ACE2 engagement by functioning as a distal "hinge." To test this possibility, chimeric Bat-SCoV genomes were constructed containing either the SARS-CoV RBM (Bat-SRBM) or the RBM plus the distal hinge residues (Bat-Hinge) (Fig. 1*B*). Electroporation yielded genome and subgenomic leader-containing transcripts at day 2, but not 5, p.e. (Fig. 1 *C* and *D*), and progeny virions could not be successfully passaged in culture.

Virus Replication in Primate and Murine Cells. We next infected Vero cells, murine delayed brain tumor (DBT) cells, and DBT cells expressing hACE2 or civet (c)ACE2 (DBT-hACE2 and DBT-cACE2) (22) with Bat-SRBD or SARS-CoV at a multiplicity of infection (MOI) of 0.01 or 1 plaque forming unit (PFU) per cell (Fig. 2). Bat-SRBD and SARS-CoV exhibited productive growth in Vero, DBT-hACE2, and DBT-cACE2 cells that was remarkably similar in kinetics and peak titers (Fig. 2). In contrast, DBT cells lacking ACE2 expression did not support growth of either SARS-CoV or Bat-SRBD (data not shown). These data indicate that Bat-SCoV expressing the SARS-CoV RBD is capable of entering cells by using ACE2 from humans, nonhuman primates, or civets as receptor, and replicating efficiently.

Detection of Bat-SRBD Replicase Proteins by SARS-CoV Antibodies. Comparison of SARS-CoV and Bat-SRBD predicted high, but not complete, identity of amino acid sequences across replicase proteins (Table S2). Because antibody cross-reactivity is a potential tool for detection and analysis of Bat-SCoVs, we tested whether antibodies specific for SARS-CoV proteins (30) could also detect Bat-SRBD homologues. Immunoblots were performed by using rabbit polyclonal antibodies (pAbs) specific for SARS-CoV nsp1, nsp8, nsp9,

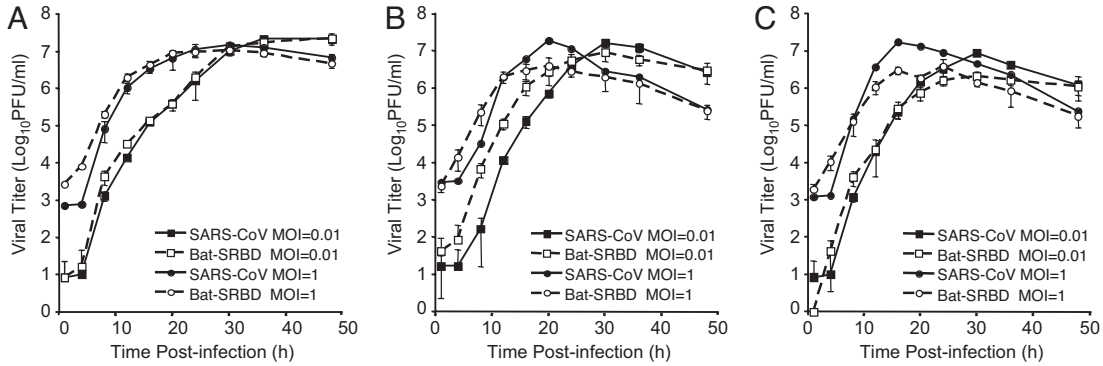

Fig. 2. Growth of SARS-CoV and Bat-SRBD in 3 different cell types. (*A–C*) Vero cells (*A*), DBT-hACE2 cells (*B*), or DBT-cACE2 cells (*C*) were infected with SARS-CoV at a MOI = 1 (■) or MOI = 0.01 (●), or Bat-SRBD at a MOI = 1 (□) or a MOI = 0.01 (○). Infected cultures were sampled, in triplicate, at the times indicated and viral titer was quantified by plaque assay on Vero cells. Error bars indicate SD.

and nsp10 (Fig. S2 and *SI Materials and Methods*). Proteins of the predicted size were detected in cells infected with SARS-CoV or Bat-SRBD demonstrating cross-reactivity of the antibodies and confirming expression of the cognate replicase proteins in Bat-SRBD.

Neutralization of Bat-SRBD. To examine antigenic relatedness, the Bat-SCoV Spike was cloned into Venezuelan Equine Encephalitis viral replicon particle (VRP) vectors, and pools of mouse (m)pAbs were tested for neutralization of Bat-SRBD infectivity. All Bat-SCoV Spike-specific sera efficiently neutralized Bat-SRBD, with 50% neutralization titers ranging from 1/100 to 1/400 dilutions (Fig. 3*A*). In parallel, these sera did not neutralize SARS-CoV infectivity, suggesting that the antibodies recognize epitopes in Spike outside the RBD in Bat-SRBD. Because the RBD appears to be the minimal motif required to alter host range of the Bat-SCoV precursor, we also tested whether Bat-SRBD could be neutralized with human monoclonal antibodies (hmAbs S109.8, S227.14, and S230.15), which recognize unique epitopes within the SARS-CoV RBD and cross-neutralize human and zoonotic SARS-CoV isolates in vitro and in vivo (31). The hmAbs neutralized Bat-SRBD, demonstrating the accessibility of the neutralizing epitopes of SRBD in the background of the Bat-SCoV Spike (Fig. 3*B*). Neutralization also functions as an important safety feature in design and study of Bat-SRBD viruses.

Bat-SRBD Replicates in Human Airway Epithelial (HAE) Cell Cultures. Because Bat-SRBD grew equivalently to SARS-CoV in culture, we tested whether Bat-SRBD could replicate in primary HAEs, which recapitulate the epithelium of the human conducting airway. We have previously identified zoonotic SARS-CoV variants that replicated efficiently in Vero cells, but not in HAE cultures (22, 32). Therefore, HAE cultures provide a more relevant and stringent measure of the replicative potential of chimeric recombinant zoonotic SARS-CoV viruses in the human host. HAE cultures were inoculated by means of the apical surface and the media sampled at different times postinfection (p.i.). Peak titers of SARS-CoV and Bat-SRBD were similar, although Bat-SRBD growth was delayed, compared with SARS-CoV (Fig. 4*A*). Because hACE2 is detected primarily on the apical surface of ciliated cells in HAEs (33), we looked for differences in targeting of Bat-SRBD and SARS-CoV infection in HAEs. Histological sections from HAE at 144-h p.i. were probed with Spike-specific antisera, and localization assessed by indirect immunofluorescence. For both viruses, Spike was detected predominantly on the apical surface of ciliated cells (Fig. 4 *B* and *C*), but was not detected in nonciliated cells.

SARS-CoV Mouse-Adapted Spike Mutation Enhances Bat-SRBD Replication in Mice. SARS-CoV replicates in mouse lungs, but causes only slight morbidity (34, 35). Replication and pathogenesis are enhanced in infections of BALB/c mice with MA15, a mouse-adapted SARS-CoV containing 6 amino acid changes, including a Y436H substitution in the Spike RBD (36). Although modeling predicts that Y436H enhances RBD-mACE2 receptor engagement (Fig. S3), both SARS-CoV and MA15 replicate efficiently in mouse lungs, complicating assignment of Y436H contributions. To test the

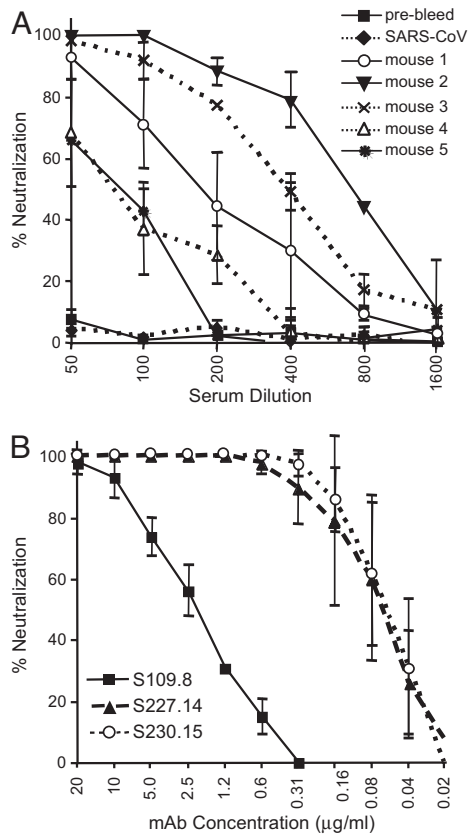

Fig. 3. Neutralization of the Bat-SRBD by mouse serum and human mAbs. (*A*) Immune sera from 5 mice (1, ○; 2, ▼; 3, ×; 4, △; and 5, ⋆) vaccinated with Bat-SCoV Spike were used to neutralize Bat-SRBD. Controls include prebleed serum (■) and Mouse 1 serum used to neutralize SARS-CoV (♦). (*B*) Human mAbs S109.8 (■), S227.14 (▲), and S230.15 (○) were used to neutralize Bat-SRBD. Results are expressed as the percentage of neutralization. Error bars indicate SD.

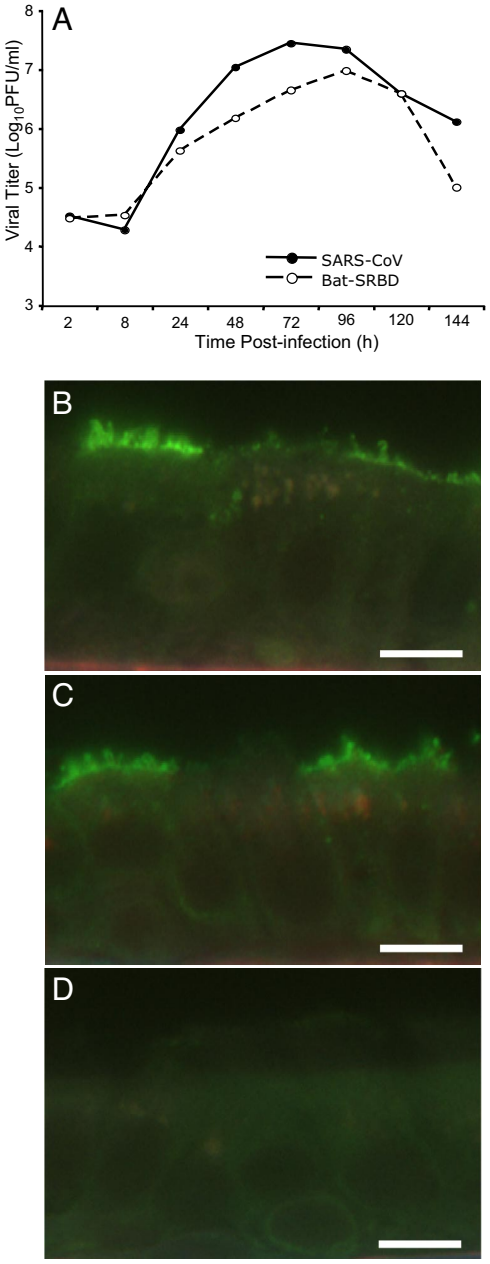

Fig. 4. Efficient replication of Bat-SRBD in human ciliated airway epithelial cells. (*A*) Growth curves for SARS-CoV and Bat-SRBD were obtained from apical washes of human ciliated airway epithelial cell cultures inoculated with either virus. Samples were serially diluted and titers determined by plaque assay on Vero cells. Titers are expressed as PFU per mL. Both SARS-CoV and Bat-SRBD replicated to titers of $\approx 10^7$, although Bat-SRBD growth was delayed compared with SARS-CoV. All inoculations were performed in duplicate. SARS-CoV, ●; Bat-SRBD, ○. (*B–D*) Representative histological sections of HAE 144 h p.i. with SARS-CoV (*B*), Bat-SRBD (*C*), or vehicle alone (*D*) and probed with mouse polyclonal sera directed against the Bat-CoV Spike and visualized with mouse-specific secondary antibodies conjugated to AlexaFluor 488 (green). Detection of Spike immunoreactivity was localized specifically to the apical surface of ciliated cells indicating that SARS-CoV and Bat-SRBD both infect ciliated cells after apical inoculation. Note that at 144 h p.i. cilial morphology shows considerable cytotoxicity. Spike immunoreactivity was not observed in nonciliated cell-types. (Scale bar, 5 μm.)

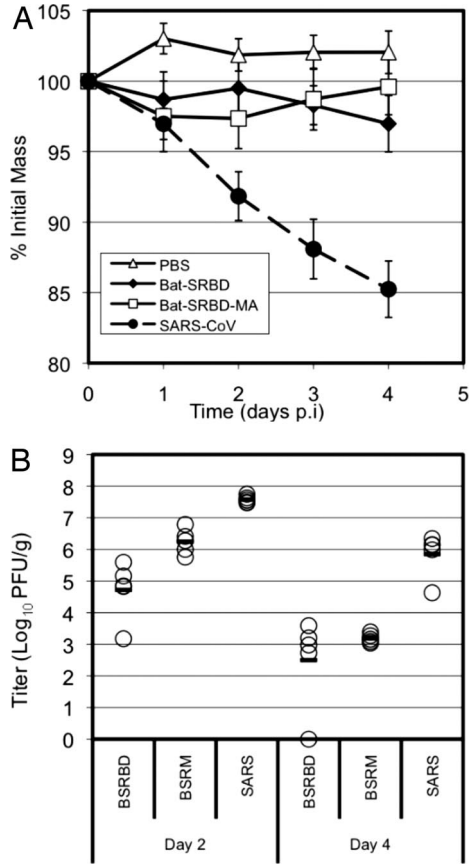

Fig. 5. Weight loss and viral replication of Bat-SRBD, Bat-SRBD-MA, and SARS-CoV in aged BALB/c mice. Ten 14-month-old female BALB/c mice were infected intranasally with 10^5 PFU of the indicated virus or an equivalent volume (50 μL) of PBS. (*A*) Weights of all surviving mice per infection group were recorded each day, averaged, and plotted as a percentage of starting weight. Error bars indicate SD. (*B*) On days 2 and 4 p.i., 5 mice per group were killed and lungs were harvested. Lung homogenates were titered on Vero cells. Circles represent titers of individual mouse lungs. Bars represent the average titer of each infection group. BSRBD, Bat-SRBD; BSRM, Bat-SRBD-MA; SARS, SARS-CoV.

hypothesis that Y436H enhances interaction with mACE2, Bat-SRBD was constructed with this substitution (Bat-SRBD-MA). Electroporation with Bat-SRBD-MA genome RNA resulted in production of infectious virus with titers similar to Bat-SRBD (Fig. 1*B*). Next, 14-month-old BALB/c mice were infected with Bat-SRBD, Bat-SRBD-MA, or SARS-CoV. Mice were weighed and monitored daily for morbidity, and on days 2 and 4 p.i., mice were euthanized and lungs harvested (Fig. 5). Mice infected with chimeric viruses did not exhibit significant weight loss or morbidity after infection (Fig. 5*A*). However, although Bat-SRBD replicated in infected lungs, Bat-SRBD-MA replicated $\approx$1.5 logs more efficiently at day 2 (Fig. 5*B*), providing support for the hypothesis that the Y436H substitution in Bat-SRBD-MA may improve mACE2 receptor engagement.

Discussion

Reverse genetic systems have revolutionized our understanding of the molecular basis of viral replication, pathogenesis, and vaccine design for many virus families. However, application of these technologies to emerging pathogens has been limited by factors involved in constructing and manipulating molecular clones and characterizing recombinant viruses, particularly those with large genomes. Also, standard approaches for development of infectious clones have required availability of viral RNA or DNA, and consequently have been mostly limited to viruses that replicate in culture. Last, classical approaches to combat emerging or deliberately introduced human pathogens may not allow responses in a timeframe adequate to significantly reduce mortality or morbidity.

Thus, new methodologies to rapidly recover and test emerging zoonotic pathogens are critical. Recent studies have provided crucial steps toward the goal of synthetic reconstruction of large microbial genomes. The 7.5- and 5.6-kb genomes of poliovirus and ϕX174, respectively, were reconstructed from known sequences by using commercially synthesized cDNA fragments and PCR assembly (37, 38). Similarly, the segmented genome of the 1918 strain of influenza was reconstructed, in part, by using synthetic design (39). Human endogenous retroviruses were assembled by PCR-directed assembly of synthetic oligonucleotides into a consensus provirus (40), and recombinant SARS-CoVs bearing synthetic zoonotic Spike sequences were derived by our group (22, 32). Last, the cloning of the 580-kb microbial genome of *Mycoplasma genitalium* was reported, although this work has not yet yielded a replicating organism (41). To our knowledge, no studies to date have used a synthetic approach to assess potential mechanisms of zoonotic emergence of a noncultivable virus.

Because it is possible that even minor events of recombination and mutation-driven evolution can alter CoV population structure and promote emergence (22, 32, 42), CoVs may select for alterations in discrete regions of Spike to achieve host-range expansion. The CoV Spike, a type I fusion protein, contains 2 discrete regions, a carboxyl-terminal S2 region that encodes fusion and heptad repeat domains in an arrangement shared by other viral attachment proteins possessing type I architecture (43), whereas the S1 region encodes the RBD. Studies in our and other laboratories have identified mutations in both S1 and S2 regions associated with CoV host-range expansion (42, 44). These 2 regions may also independently or cooperatively mediate transspecies expansion and neutralization escape, in that some mAbs that target the SARS-CoV S1 RBD select for escape mutants in the RBD, but also in the S2 region (45). These data suggest that coordinated interactions between the S1 RBD and select S2 domains may be important in epitope presentation and Spike function.

We have identified several hmAbs that bind distinct, conserved locations in the SARS-CoV RBD and neutralize strains that originate from animal and human hosts (31). These hmAbs did efficiently neutralize Bat-SRBD, an important finding as it was not previously clear that mAbs targeting the SARS-CoV RBD would neutralize virus in the context of a different Spike backbone. It is also informative that antibodies specific for the Bat-SCoV Spike protein neutralize Bat-SBRD, which expresses a chimeric Spike protein, but not SARS-CoV, indicating the existence of neutralizing antibodies that target portions of Spike outside the RBD. Importantly, these results suggest that hmAbs specific for SARS-CoV, and by inference the current panel of SARS-CoV vaccines, may provide significant protection against other SARS-like CoVs that emerge from zoonotic pools by natural recombination or are deliberately designed to cross species. Second, both SARS-CoV RBD-specific hmAbs and Bat-SCoV mpAbs specific for Spike epitopes outside of the RBD are able to recognize and neutralize virus even in the setting of a chimeric Spike, providing important safety features for studies of emerging zoonotic CoVs.

It has been shown that the 5′ UTRs of CoVs can influence the capacity of the virus to replicate in cells (46). Although the 5′ UTR in the synthetic Bat-SCoV originated from SARS-CoV, the sole difference between Bat-SCoV, which was not capable of amplification in cell culture, and Bat-SRBD, which could be recovered, was the RBD derived from SARS-CoV. Our results also confirm and extend a previous report predicting that deletions and mutations within the Bat-SCoV RBM ablate interaction with hACE2 and cACE2 molecules (47). Thus, in this report, we show that the CoV Spike RBD is interchangeable, is sufficient to confer efficient growth and infectivity in cells from multiple species, and likely represents a critical determinant of transspecies movement of zoonotic CoVs.

To protect against future emerging zoonotic pathogens, it is crucial to develop cell culture and animal models to test vaccines and therapeutics, ideally against entire families of organisms, such as CoVs. Both SARS-CoV and Bat-SRBD replicated efficiently in HAE cultures, providing a direct human airway model for comparison of existing and new antivirals. However, Bat-SRBD replicated poorly in vivo, calling for additional modifications to facilitate studies in mouse models. Robust structural information exists on the RBD-ACE2 interaction (29), mutations affecting this interaction have been identified (22, 31), and Rosetta-modeling of short range RBD-mACE2 receptor interfaces can identify key residues essential for retargeting the host specificity of Bat-SRBD (Fig. S3) (48). Previous studies had identified a mutation in the RBD of the MA15 strain, Y436H, but its exact role in vivo was not clear (36). By using structural modeling algorithms, we predicted that the Y436H substitution would enhance the interaction of Bat-SRBD with mACE2. Bat-SRBD-MA did exhibit increased growth efficiency in aged mice. However, this did not result in clinical disease, suggesting the requirement for additional adaptive changes. For example, SARS-CoV encodes at least 5 IFN antagonists, predicted to function in virulence (49–52). Our model system will allow mapping of the domains in the Bat-SCoV and SARS-CoV genetic backgrounds involved in regulation of virulence in aged animals.

In this report, sequence and structural information was integrated with synthetic genomics, reverse genetics, and protein design to recover a zoonotic precursor virus from a hypothetical infectious sequence. The resulting chimera exhibited cross-reactivity with previously identified therapeutics and highlighted possible previously undescribed mechanisms for host-range expansion. Here, we articulate a model to predict and directly test tenable emergence pathways. Paired with a greater availability of reagents and therapeutics, our studies represent an approach for rapid recovery and testing of newly identified pathogens, and which may improve public health preparedness and intervention strategies against natural or intentional zoonotic-human epidemics.

Materials and Methods

Cells and Viruses. VeroE6 cells (Vero) were maintained in MEM (Invitrogen), and delayed brain tumor (DBT, murine astrocytoma) cells were maintained in Dulbecco's MEM (Invitrogen) containing 10% FBS. DBT-hACE2 and DBT-cACE2 cells were cultured as described (22). HAE cells were plated and differentiated as described (33). SARS-CoV Urbani strain (hereafter, SARS-CoV) and Bat-SCoV wild type and chimeric viruses were propagated and assessed by plaque assay on Vero cells. All studies with viable SARS-CoV and SARS-CoV-like viruses were performed in certified BSL3 laboratories in biological safety cabinets, by using safety protocols that were reviewed and approved by the Institutional Biosafety Committees of Vanderbilt University and the University of North Carolina at Chapel Hill.

Determining the Consensus Sequence for Synthetic Bat-SCoV and Conceptual Design of the Bat-SCoV Clone. HKU3–1 (DQ022305), HKU3–2 (DQ084200), HKU3–3 (DQ084199), and RP3 (DQ071615) genomes were aligned by using ClustalXv1.83 to determine a consensus sequence (Fig. S1 and Figs. S4–S6) (GenBank accession no. FJ211859). The consensus Bat-SCoV sequence was designed to ligate interchangeably with the SARS-CoV infectious clone (24). Notably, there was no consensus at the 5′end of the Bat-SCoV genomes, so we used the 5′ most region of SARS-CoV to append the T7 promoter site to the 5′ end of the Bat-A fragment.

Construction of Chimeric Spike Variants. Insertions of SARS-CoV sequence in place of Bat-SCoV sequence were engineered by using PCR and the primers shown in Table S3. PCR amplicons for Bat-SRBD (GenBank accession no. FJ211860) and Bat-SRBM were generated by using fragments Bat-E2, and SARS-E. PCR amplicons for Bat-Hinge (Bat-SRBM plus 6 additional residues from SARS-CoV Spike) were generated by using Bat-SRBM as template. PCR-generated products were cloned into the Bat-E2 plasmid by using unique 5′-BstBI and 3′-MscI sites. Successful insertions of SARS-CoV sequence were confirmed by restriction digestion and nucleotide sequencing across the region of PCR amplification.

Generation of SARS-CoV and Bat-SCoV Mutant Viruses. Viruses containing PCR-generated insertions within the viral coding sequence were produced by using the SARS-CoV assembly strategy (24, 33, 53) with the following modifications. Briefly, for Bat-F virus, full-length cDNA was constructed by ligating restriction products from SARS-CoV fragments A–E and Bat-SCoV fragment F, which required a BglI-NotI digestion. For Bat-SCoV and Bat-SRBD, Bat-SRBM, and Bat-

Hinge, plasmids containing the 7 cDNA fragments of the Bat-SCoV genome were digested by using BglI for Bat-A, Bat-B, Bat-C, and Bat-D, BglI and AflII for Bat-E1 and Bat-E2, and BglI and NotI for Bat-F. Digested, gel-purified fragments were simultaneously ligated together. Transcription was driven by using a T7 mMessage mMachine kit (Ambion), and RNA was electroporated into Vero cells (24, 53). Virus viability was determined by cytopathic effect and progeny viruses were passaged at low MOI. RNA was recovered from infected cell monolayers by using TRIzol (Invitrogen) according to the manufacturer's instructions, and genome origins were verified by RT-PCR and nucleotide sequencing.

Assay for Bat-SCoV Leader-Containing Transcripts in Electroporated Cells and Mouse Lungs. At days 2 and 5 p.e., generation of leader-containing N (ORF9) and genome (ORF1) transcripts was determined by RT-PCR. Briefly, RT-PCR was performed by using random hexamers (ABI) and SuperScript III (Invitrogen) to generate first-strand cDNA at an extension temperature of 55 °C for 1 h. Leader-containing cDNAs were amplified by PCR by using Taq with Thermopol buffer (NEB) and the following primers: 5′-CAGGAAAAGCCAACCAACCTTG (leader) and 5′-CGCTACGACCGAACTGAATGCC to detect Bat-SCoV genomic RNA; and leader and 5′-GTGAGAGCTGTGAACCAAGACG to detect mRNA 9 transcripts. Presence or absence of PCR products was assessed by electrophoresis on 1.5% agarose gels.

Viral Growth and Plaque Assays. Vero, DBT, DBT-hACE2, or DBT-cACE2 cells were infected at a MOI of 1 or 0.01 PFU/cell. After 1 h at 37 °C, the inocula were removed, cells were washed and samples were taken at different times p.i. To determine viral titer, samples were diluted, inoculated onto Vero cell monolayers in 6-well plates for 1 h, and overlaid with complete media plus 1% agar. Plaques were visualized between 48 and 52 h p.i. by neutral red staining (Sigma).

Generation of Polyclonal Bat-SCoV Spike-Specific Sera and Neutralization Assay. Murine pAbs specific for the Bat-SCoV Spike were generated as previously described (33). Neutralizing titers for mpAbs and hmAbs S109.8, S227.14, and S230.15 were determined by plaque reduction neutralization titer assay (PRNT50%) (31). The percentage of neutralization was calculated as follows: 1-(number of plaques in the presence of antibody/number of plaques in the absence of antibody) x 100%.

Infection of Aged BALB/c Mice. Ten each of aged (14 months) female BALB/c mice (National Institute of Aging) were lightly anesthetized and infected intranasally with 10^5 PFU of Bat-SRBD, Bat-SRBD-MA, or SARS-CoV; 5 additional mice were inoculated with an equivalent volume (50 μL) of PBS. Mice were weighed daily through 4 days p.i., and on days 2 and 4 p.i., 5 mice of each group were killed and lungs harvested for determination of viral titer. Lungs were weighed and homogenized in 500 μL of PBS at 6,000 rpm for 60 s in a MagnaLyser (Roche). Clarified homogenates were then diluted serially, and titers were determined by plaque assay on Vero cells.

ACKNOWLEDGMENTS. We thank XiaoTao Lu and Sunny Lee for technical assistance, Susan Burkett for maintenance of the HAE cultures, Perry Myrick for immunofluorescence assays, and the University of North Carolina Cystic Fibrosis Tissue Culture Core for HAE cells. M.M.B., R.L.G., R.S.B., and M.R.D. are supported by the National Institute of Allergy and Infectious Diseases Public Health Service Award P01 AI59943. Additional support was provided by Public Health Service Award CA68485 to the Vanderbilt University DNA Sequencing Shared Resource of the Vanderbilt–Ingram Cancer Center. The Baric laboratory is supported by the Gillings Innovation Fund.

1. Weiss RA, McMichael AJ (2004) Social and environmental risk factors in the emergence of infectious diseases. *Nat Med* 10:S70–76.
2. Woolhouse ME, Gowtage-Sequeria S (2005) Host range and emerging and reemerging pathogens. *Emerg Infect Dis* 11:1842–1847.
3. Webby R, Hoffmann E, Webster R (2004) Molecular constraints to interspecies transmission of viral pathogens. *Nat Med* 10:S77–81.
4. Drosten C, *et al.* (2003) Identification of a novel coronavirus in patients with severe acute respiratory syndrome. *N Engl J Med* 348:1967–1976.
5. Ksiazek TG, *et al.* (2003) A novel coronavirus associated with severe acute respiratory syndrome. *N Engl J Med* 348:1953–1966.
6. Peiris JS, *et al.* (2003) Coronavirus as a possible cause of severe acute respiratory syndrome. *Lancet* 361:1319–1325.
7. Tu C, *et al.* (2004) Antibodies to SARS coronavirus in civets. *Emerg Infect Dis* 10:2244–2248.
8. Kan B, *et al.* (2005) Molecular evolution analysis and geographic investigation of severe acute respiratory syndrome coronavirus-like virus in palm civets at an animal market and on farms. *J Virol* 79:11892–11900.
9. Guan Y, *et al.* (2003) Isolation and characterization of viruses related to the SARS coronavirus from animals in southern China. *Science* 302:276–278.
10. Li W, *et al.* (2005) Bats are natural reservoirs of SARS-like coronaviruses. *Science* 310:676–679.
11. Shi Z, Hu Z (2008) A review of studies on animal reservoirs of the SARS coronavirus. *Virus Res* 133:74–87.
12. Lau SK, *et al.* (2005) Severe acute respiratory syndrome coronavirus-like virus in Chinese horseshoe bats. *Proc Natl Acad Sci USA* 102:14040–14045.
13. Dominguez SR, O'Shea TJ, Oko LM, Holmes KV (2007) Detection of group 1 coronaviruses in bats in North America. *Emerg Infect Dis* 13:1295–1300.
14. Halpin K, *et al.* (2007) Emerging viruses: Coming in on a wrinkled wing and a prayer. *Clin Infect Dis* 44:711–717.
15. Calisher CH, *et al.* (2006) Bats: Important reservoir hosts of emerging viruses. *Clin Microbiol Rev* 19:531–545.
16. Holmes EC, Rambaut A (2004) Viral evolution and the emergence of SARS coronavirus. *Philos Trans R Soc Lond B Biol Sci* 359:1059–1065.
17. Lai MM, Cavanagh D (1997) The molecular biology of coronaviruses. *Adv Virus Res* 48:1–100.
18. Stavrinides J, Guttman DS (2004) Mosaic evolution of the severe acute respiratory syndrome coronavirus. *J Virol* 78:76–82.
19. Li W, *et al.* (2006) Animal origins of the severe acute respiratory syndrome coronavirus: Insight from ACE2-S-protein interactions. *J Virol* 80:4211–4219.
20. Li W, *et al.* (2007) The S proteins of human coronavirus NL63 and severe acute respiratory syndrome coronavirus bind overlapping regions of ACE2. *Virology* 367:367–374.
21. Li W, *et al.* (2005) Receptor and viral determinants of SARS-coronavirus adaptation to human ACE2. *EMBO J* 24:1634–1643.
22. Sheahan T, *et al.* (2008) Mechanisms of zoonotic severe acute respiratory syndrome coronavirus host range expansion in human airway epithelium. *J Virol* 82:2274–2285.
23. Pruitt KD, Tatusova T, Maglott DR (2003) NCBI Reference Sequence project: Update and current status. *Nucleic Acids Res* 31:34–37.
24. Yount B, *et al.* (2003) Reverse genetics with a full-length infectious cDNA of severe acute respiratory syndrome coronavirus. *Proc Natl Acad Sci USA* 100:12995–13000.
25. Kuo L, *et al.* (2000) Retargeting of coronavirus by substitution of the spike glycoprotein ectodomain: Crossing the host cell species barrier. *J Virol* 74:1393–1406.
26. Haijema BJ, Volders H, Rottier PJ (2003) Switching species tropism: An effective way to manipulate the feline coronavirus genome. *J Virol* 77:4528–4538.
27. Chakraborti S, Prabakaran P, Xiao X, Dimitrov DS (2005) The SARS coronavirus S glycoprotein receptor binding domain: Fine mapping and functional characterization. *Virol J* 2:73.
28. Wong SK, *et al.* (2004) A 193-amino acid fragment of the SARS coronavirus S protein efficiently binds angiotensin-converting enzyme 2. *J Biol Chem* 279:3197–3201.
29. Li F, Li W, Farzan M, Harrison SC (2005) Structure of SARS coronavirus spike receptor-binding domain complexed with receptor. *Science* 309:1864–1868.
30. Prentice E, *et al.* (2004) Identification and characterization of severe acute respiratory syndrome coronavirus replicase proteins. *J Virol* 78:9977–9986.
31. Rockx B, *et al.* (2008) Structural basis for potent cross-neutralizing human monoclonal antibody protection against lethal human and zoonotic severe acute respiratory syndrome coronavirus challenge. *J Virol* 82:3220–3235.
32. Rockx B, *et al.* (2007) Synthetic reconstruction of zoonotic and early human severe acute respiratory syndrome coronavirus isolates that produce fatal disease in aged mice. *J Virol* 81:7410–7423.
33. Sims AC, *et al.* (2005) Severe acute respiratory syndrome coronavirus infection of human ciliated airway epithelia: Role of ciliated cells in viral spread in the conducting airways of the lungs. *J Virol* 79:15511–15524.
34. Subbarao K, Roberts A (2006) Is there an ideal animal model for SARS? *Trends Microbiol* 14:299–303.
35. Roberts A, *et al.* (2008) Animal models and vaccines for SARS-CoV infection. *Virus Res* 133:20–32.
36. Roberts A, *et al.* (2007) A mouse-adapted SARS-coronavirus causes disease and mortality in BALB/c mice. *PLoS Pathog* 3:e5.
37. Smith HO, Hutchison CA, III, Pfannkoch C, Venter JC (2003) Generating a synthetic genome by whole genome assembly: PhiX174 bacteriophage from synthetic oligonucleotides. *Proc Natl Acad Sci USA* 100:15440–15445.
38. Cello J, Paul AV, Wimmer E (2002) Chemical synthesis of poliovirus cDNA: Generation of infectious virus in the absence of natural template. *Science* 297:1016–1018.
39. Tumpey TM, *et al.* (2005) Characterization of the reconstructed 1918 Spanish influenza pandemic virus. *Science* 310:77–80.
40. Lee YN, Bieniasz PD (2007) Reconstitution of an infectious human endogenous retrovirus. *PLoS Pathog* 3:e10.
41. Gibson DG, *et al.* (2008) Complete chemical synthesis, assembly, and cloning of a Mycoplasma genitalium genome. *Science* 319:1215–1220.
42. McRoy WC, Baric RS (2008) Amino acid substitutions in the S2 subunit of mouse hepatitis virus variant V51 encode determinants of host range expansion. *J Virol* 82:1414–1424.
43. Lamb RA, Jardetzky TS (2007) Structural basis of viral invasion: Lessons from paramyxovirus F. *Curr Opin Struct Biol* 17:427–436.
44. Schickli JH, Thackray LB, Sawicki SG, Holmes KV (2004) The N-terminal region of the murine coronavirus spike glycoprotein is associated with the extended host range of viruses from persistently infected murine cells. *J Virol* 78:9073–9083.
45. Mitsuki YY, *et al.* (2008) A single amino acid substitution in the S1 and S2 Spike protein domains determines the neutralization escape phenotype of SARS-CoV. *Microbes Infect* 10:908–915.
46. Hofmann MA, Senanayake SD, Brian DA (1993) A translation-attenuating intraleader open reading frame is selected on coronavirus mRNAs during persistent infection. *Proc Natl Acad Sci USA* 90:11733–11737.
47. Ren W, *et al.* (2008) Difference in receptor usage between severe acute respiratory syndrome (SARS) coronavirus and SARS-like coronavirus of bat origin. *J Virol* 82:1899–1907.
48. Li W, *et al.* (2004) Efficient replication of severe acute respiratory syndrome coronavirus in mouse cells is limited by murine angiotensin-converting enzyme 2. *J Virol* 78:11429–11433.
49. Kopecky-Bromberg SA, *et al.* (2007) Severe acute respiratory syndrome coronavirus open reading frame (ORF) 3b, ORF 6, and nucleocapsid proteins function as interferon antagonists. *J Virol* 81:548–557.
50. Kopecky-Bromberg SA, Martinez-Sobrido L, Palese P (2006) 7a protein of severe acute respiratory syndrome coronavirus inhibits cellular protein synthesis and activates p38 mitogen-activated protein kinase. *J Virol* 80:785–793.
51. Frieman M, *et al.* (2007) Severe acute respiratory syndrome coronavirus ORF6 antagonizes STAT1 function by sequestering nuclear import factors on the rough endoplasmic reticulum/Golgi membrane. *J Virol* 81:9812–9824.
52. Wathelet MG, Orr M, Frieman MB, Baric RS (2007) Severe acute respiratory syndrome coronavirus evades antiviral signaling: Role of nsp1 and rational design of an attenuated strain. *J Virol* 81:11620–11633.
53. Graham RL, *et al.* (2005) The nsp2 replicase proteins of murine hepatitis virus and severe acute respiratory syndrome coronavirus are dispensable for viral replication. *J Virol* 79:13399–13411.